THE ASTRONOMICAL JOURNAL, 120:1612–1625, 2000 October

RADIO GALAXY–SELECTED CLUSTERS AT HIGH REDSHIFT AND ASSOCIATED EXTREMELY RED OBJECT OVERDENSITIES

S. C. CHAPMAN, P. J. MCCARTHY, AND S. E. PERSSON
Observatories of the Carnegie Institution of Washington, 813 Santa Barbara Street, Pasadena, CA 91101
Received 2000 May 16; accepted 2000 June 14

ABSTRACT

Galaxy clusters at high redshift present a superb opportunity to study galaxy evolution, with large galaxy samples at fixed distances. Several lines of evidence point toward large formation redshifts and passive evolution for cluster elliptical galaxies. At redshifts higher than $z \sim 0.8$, this picture rests on data from only a handful of rich clusters. We have observed four potential clusters to sample sparser environments in a critical redshift range, $0.8 < z < 1.2$. We compare the photometric evolution and radial density profiles in our clusters with more massive clusters studied in a similar manner. We also highlight the overdense extremely red object ($I-K > 5$) population, significantly redder than the old elliptical population at the cluster redshift. We discuss the implications of our clusters at high redshift and possible differences in environment from richer clusters at similar redshifts selected through X-ray or optical techniques.

Key words: galaxies: clusters: general — galaxies: evolution — galaxies: formation — infrared radiation — radio emission lines

1. INTRODUCTION

High-redshift galaxy clusters present luminous signposts for the formation and evolution of massive galaxies. While the study of field galaxies at very high redshifts ($z > 3$) has recently progressed (e.g., Steidel et al. 1999), clusters continue to be our best probe of dense environments and large mass scales at early epochs. Clusters with luminous active galactic nuclei (AGNs) at their centers offer a different perspective on galaxy interactions and activity than clusters selected either on the basis of optical overdensities or spatially extended X-ray emission. The AGN-selected clusters tend to be poorer than the optically and X-ray–selected rich clusters that dominate most catalogs and, thus, probe a different range of environments (Lilly & Prestage 1987). Such a sparse environment may also be related to the formation and fueling of the luminous AGN (Heckman et al. 1986).

The existence of massive collapsed objects, particularly rich galaxy clusters, at high redshifts provides a challenge for theories of cosmic structure formation (e.g., Press & Schechter 1974). The $z \sim 1$ range represents a critical point at which serious constraints can be placed on the formation and evolutionary history of early-type galaxies in clusters. Beyond $z \sim 1$ in cosmologically flat cold dark matter models, the amount of merging occurring within the prior ~ 1 Gyr was thought to be sufficiently large so as to dramatically inflate the locus of early-type galaxy colors. Recent modeling has shown however that the locus of such red galaxies may remain quite tight until beyond $z \sim 1.5$ (Kauffmann & Charlot 1998). However, these models still have difficulty predicting the correct slope of the red sequence.

The emerging evolutionary picture from the study of a few high-redshift galaxy clusters (e.g., Ellis et al. 1997; Stanford, Eisenhardt, & Dickinson 1998; Kodama et al. 1998) is one of smooth and steady spectrophotometric evolution for early-type galaxies over more than half the age of the universe—implying large formation redshifts and primarily passive evolution. The average E+S0 galaxy color at a particular luminosity evolves gradually, while both the slope and scatter of galaxy colors around the mean change very little. The small scatter implies that, even approaching $z \sim 1$, we have not reached the time at which a significant fraction of the stars in early-type galaxies were young. The fact that the color-magnitude slope does not change with redshift strongly favors a scenario in which this slope arises from a mass-metallicity correlation (Stanford et al. 1998). Different burst ages and epochs would result in a changing slope with redshift.

The evolution of luminous AGNs may be tied to the evolution of their parent environments, particularly in clusters. The peak in the QSO luminosity evolution is thought to have occurred within $1 < z < 3$ (e.g., Boyle & Terlevich 1998). This was *the age* of quasars. In the present epoch, powerful AGNs are far less numerous and appear not to inhabit very overdense regions. However, prior to $z \sim 0.5$ conditions were different; many radio-loud AGNs existed in overdense or cluster environments (see, e.g., Hall & Green 1998; Yates, Miller, & Peacock 1989; Yee & Green 1984; Hill & Lilly 1991; Ellingson, Yee, & Green 1991). If mergers and interactions are indeed the key to fueling luminous AGNs, then the temperatures and velocity dispersions in later epoch clusters ($z \sim 0$) may be too large for efficient mass transport. The strong QSO evolution may be naturally explained as a result of cluster virialization and evolution—at higher redshift, the lower galaxy velocities lead to higher interaction probabilities (see, e.g., Fabian & Crawford 1990). A luminous AGN present at the cluster center may be an indicator of rapid dynamical evolution of the cluster and the constituent galaxies.

Although a few recent studies have addressed cluster elliptical galaxy evolution at redshifts ~ 1 (Stanford et al. 1997, 1998; Rosati et al. 1999; Tanaka et al. 2000; Kajisawa et al. 2000), there is a marked paucity of data available for clusters in this critical redshift regime ($z \sim 1$), especially those with less rich environments, where mergers are expected to be more efficient. We have identified a sample of potential high-redshift clusters from a complete sample of radio galaxies (Chapman & McCarthy 2000), the Molonglo Reference Catalog 1 Jy sample (McCarthy et al.

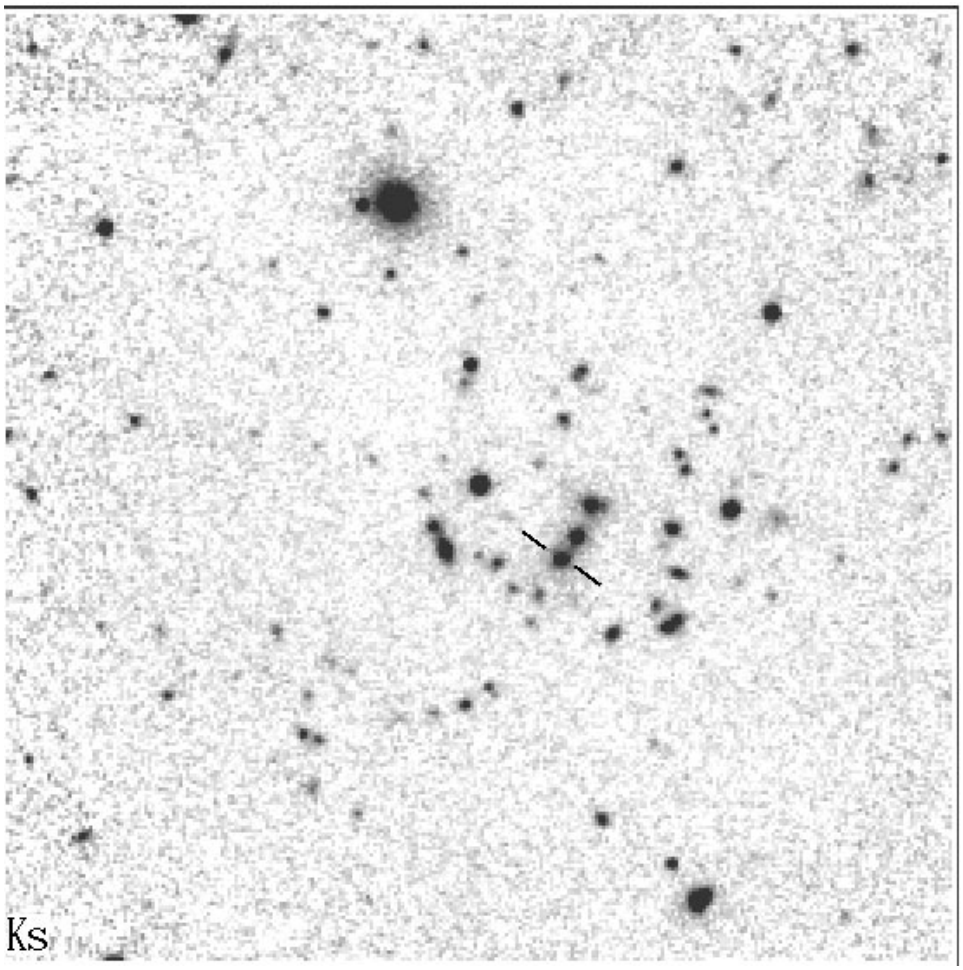

FIG. 1*a*

FIG. 1.—Cluster field images comparing the near-IR with the optical: MRC 0527−255 (*a*) *K* and (*b*) *V*; field size 95″ on a side. The radio galaxy is marked in the K_s-band images. In all fields in this paper, north is up, east is left.

TABLE 1

PROPERTIES OF THE RADIO GALAXY CLUSTERS

Property	MRC 0527−255	MRC 0959−263	MRC 1022−299	MRC 1139−285
4 σ limit:				
K_s	20.5	20.3	20.5	20.4
H	21.2	…	21.3	…
J	21.0	…	21.4	…
I	24.6	24.4	24.5	24.5
V	25.5	24.6[a]	25.5	25.2
Redshift:				
Radio galaxy	…	0.68 ± 0.005	0.93 ± 0.005	0.85 ± 0.005
Red sequence	1.28 ± 0.03	0.75 ± 0.02	0.94 ± 0.02	0.77 ± 0.02
Abell class	1.5	1.5	2	1
Red galaxies:				
$R < 10''$	6	5	3	2
$R < 35''$	22	13	16	9
$R < 60''$	32	31	38	20
EROs to $K = 20.0$ (20.7):				
$I-K > 5$	3 (6)	3 (5)	2 (3)	2 (6)
> Red seq. + 1 mag	4 (10)	3 (7)	4 (5)	3 (8)
$S_{408\ \mathrm{MHz}}$ (mJy)	1540	1720	1120	6810
$\alpha_{843/408}$	0.88	0.82	0.84	0.85
Radio structural type	Partly resolved	Triple source	Partly resolved	Double source

[a] Has Gunn *r* magnitude rather than *V*.

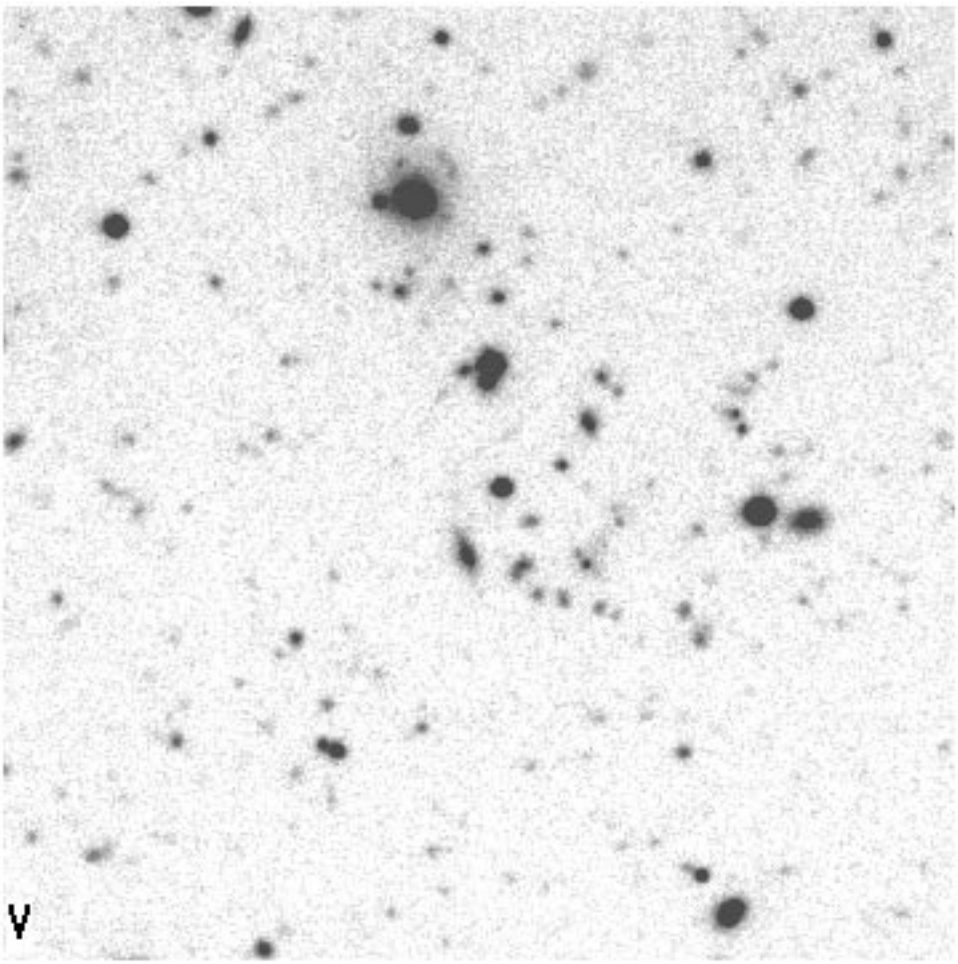

FIG. 1*b*

1996; Kapahi et al. 1998). We have selected all sources identified with galaxies with measured redshifts in the range $0.8 < z < 1.5$, using visible and K_s-band images obtained with the 2.5 m du Pont Telescope at Las Campanas. Since old elliptical cluster galaxies have very red colors, K-band galaxy selection removes a large source of blue interloping field galaxies, highlighting potential cluster members. In addition, cluster members do not suffer as greatly from k-corrections in the K band as in the optical (Stanford et al. 1998), and K-magnitude/color diagrams therefore present a comparable study of cluster evolution across a range of redshifts.

In this paper, we present deep multiband images of four obviously overdense radio galaxy fields from our sample at $z > 0.8$. Confirming the cluster status will ultimately require spectroscopic measurements of redshift for many cluster members. With the present data, we rely on color-magnitude diagram (CMD) analyses to reveal the characteristic red sequence of elliptical cluster members, in consort with the measured radio galaxy redshift and, in one case (MRC 0959−263), a few cluster member redshifts lying fortuitously along the slit (§§ 3.1, 3.2). A radial density analysis is also used to assess the cluster richness over the field population (§ 3.3). We also highlight the overdense extremely red object (ERO) population, significantly redder than the old elliptical population at the cluster redshift (§ 3.4). In § 4, we discuss the implications of our clusters at high redshift and possible differences in environment from richer clusters at similar redshifts selected though X-ray or optical techniques.

2. THE SAMPLE, OBSERVATIONS, AND REDUCTION

The four radio galaxy fields in this study were chosen from a large sample of K- and V-band images, because of an apparent overdensity of red galaxies in the K image when compared with V. We also required that the $V-K$ versus K CMD reveal a linear sequence of red galaxies including the radio galaxy as further evidence for the cluster environment. This was not meant to be systematic for the sample but merely to choose a few potential clusters at $z \sim 1$ for deeper follow-up observations.

2.1. *Imaging*

The optical and near-IR images on which our present analysis is based were obtained using the 100 inch (2.5 m) du Pont Telescope at Las Campanas, Chile, using CCD cameras in the optical. The J- and H-band images were obtained with the CIRSI camera (Beckett et al. 1998; 1K × 1K pixel HAWAII array), while the K_s-band images were taken with IRCAM (Persson et al. 1992; NICMOS3 array). The details of the optical observations and their reduction can be found in McCarthy et al. (1996). The near-IR observations were taken with a 30″ dither pattern and reduced in a standard approach for IR imaging.

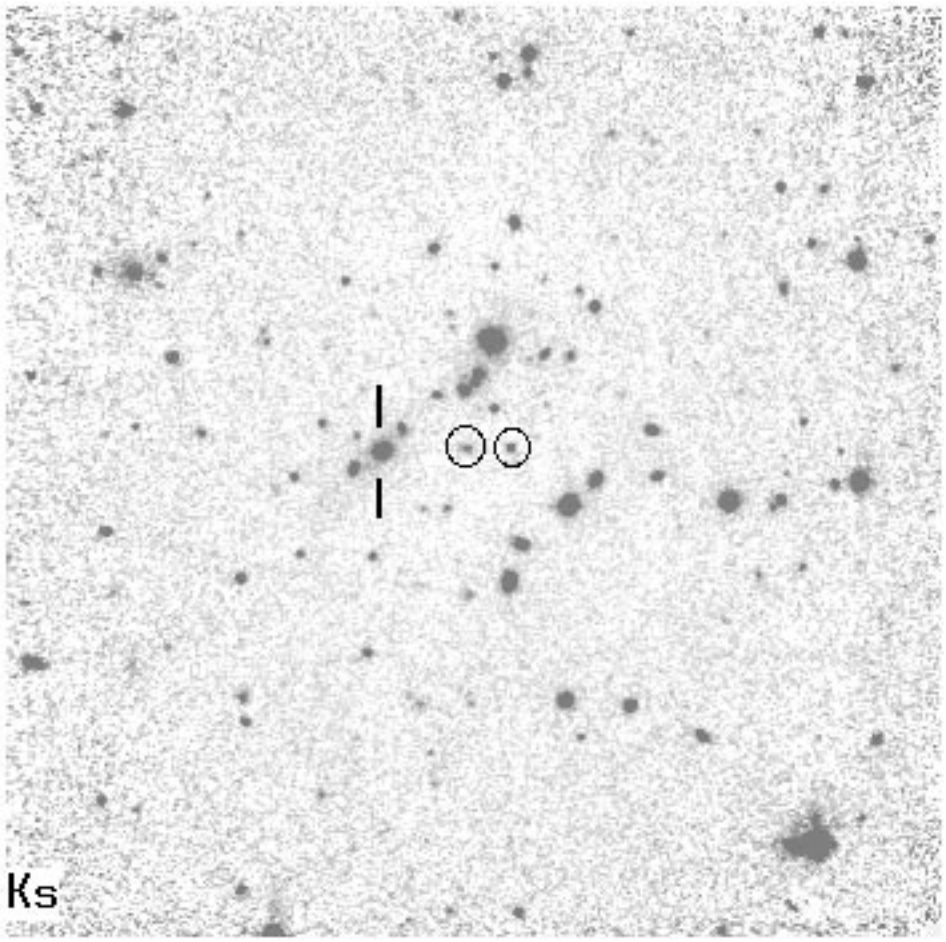

FIG. 2*a*

FIG. 2.—Same as Fig. 1, but for MRC 0959−263 (*a*) *K* and (*b*) *I*; field size 110″ on a side. The other cluster members with confirmed redshifts are circled.

To facilitate the analysis of the data sets, the various images of the four cluster fields were resampled and rotated to common reference frames using the IRAF tasks GEOMAP and GEOTRAN. The fields are centered on the initial estimate of the cluster positions from the red galaxy spatial distribution. The final images have the same pixel size as the 0.″265 pixel^{-1} CCD images.

The source extraction software SExtractor (Bertin & Arnouts 1996) was used to make an initial object detection pass at greater than 3 σ, with the final catalog at greater than 4 σ in the K_s-band images, while measuring flux parameters for each individual passband in the separate images. Magnitudes and colors were measured using a 2″ diameter aperture, roughly twice the FWHM of the images. The depths reached in each filter vary somewhat field to field but are typically close to 4 σ detection limits of K_s = 20.5, H = 21.4, J = 21.4, I = 24.0, and V = 25.0. The actual limits for each field are presented in Table 1. Figures 1–4 present the near-IR and optical images of the four clusters, while Figure 5 depicts a false-color image of the richest cluster in our sample, MRC 1022−299. For visualization, an $I-K$ representation of each field is presented in Figure 6, with squares highlighting probable cluster members (those lying within the presumed locus of early-type galaxies, as discussed in the next section).

The Galactic $E(B-V)$ toward the four fields is small ($\approx$0.04), and we have not applied an extinction correction to our photometry. We estimate the quadrature sum of the systematic 1 σ errors in the photometry (zero points and point-spread function matching) to be $\sim$0.05 for the IR colors and $\sim$0.04 for the optical-K colors.

2.2. *CTIO* 4 m *Spectroscopy*

The Ritchey-Chrétien spectrograph on the CTIO 4 m telescope was used to obtain optical spectra for the four radio galaxies, although no clear redshift was measured for MRC 0527−255. For MRC 0959−263, two other galaxies falling on the slit had redshifts within 5% of the radio galaxy and are likely cluster members. Details of the observations and reductions can be found in McCarthy, Elston, & Eisenhardt (1992), while the spectra will be presented in McCarthy et al. (2000)

3. ANALYSIS AND RESULTS

3.1. *Color-Magnitude Diagram Analysis*

The CMD forms our main diagnostic for identifying red galaxy overdensities, and we present a brief overview of the technique before discussing each cluster individually. The CMD for a galaxy cluster typically reveals a tight red sequence of massive elliptical galaxies, implying a mass-metallicity relation for early-type cluster galaxies (Stanford et al. 1998; Gladders et al. 1998). This argument can be inverted to search for the presence of a cluster via the red

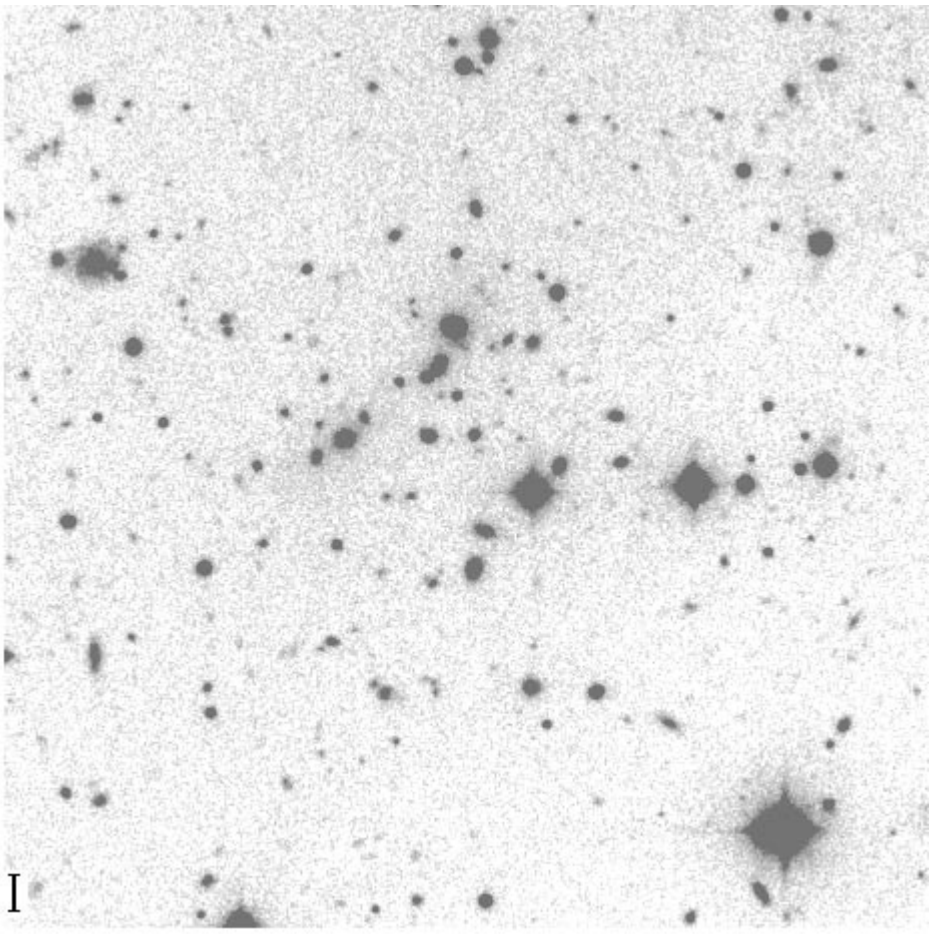

FIG. 2*b*

elliptical sequence. The fact that studies to date have implied large formation redshifts and primarily passive evolution for the cluster elliptical galaxies allows the red sequence to be used as an estimate of the cluster redshift, even at redshifts out to $z \sim 1$. We have used this approach to characterize the environments of the four radio galaxies under investigation here. In the cases where the radio galaxy redshift is known, we have, along with $z_{\rm CMD}$, two independent measures of the cluster redshift to compare.

Figure 7 shows the CMDs for the radio galaxy fields in observed-frame colors. For the two higher redshift clusters, *J*- and *H*-band images were obtained since the near-IR colors begin to show a significant deviation from the field population. Two radial cuts have been made on the object catalog centered on the radio galaxy, with squares representing objects within 35″ of the radio galaxy, crosses those from 35″ to 60″, and circles objects greater than 60″. The solid diagonal lines represent 4 σ detection thresholds in color. A color-magnitude sequence of red galaxies, which includes the radio galaxy, is visible in Figure 7 for all clusters, with many of the red objects lying within the central 35″. Our position-color representations of the cluster fields (Fig. 6) depict the red-sequence objects with squares, while triangles depict bluer objects lying below the red sequence.

Plotted in all panels of Figure 7 (*dashed lines*) are estimates of the no-evolution color-magnitude locus for early-type galaxies. These are derived from the data set described by Stanford et al. (1998), which uses multiband photometry of early-type galaxies covering the central $\sim$1 Mpc of the Coma Cluster (Eisenhardt & De Propris 1997; Stanford et al. 1998). The dashed lines therefore represent the colors that Coma galaxies would appear to have if the cluster could be placed at the redshifts of our radio galaxies and observed through the $VRIJHK_s$ filters we used. The dashed lines were interpolated from the values presented in Stanford et al. (1998), where they have a cluster very near the redshift of each cluster in our sample to $z = 1$. For MRC 0527$-$255, we made a very small extrapolation to the no-evolution Coma line from the Lynx field clusters at $z = 1.26$ presented by Rosati et al. (1998) and Stanford et al. (1997).

Our procedure was to fit a line to all objects within $18 < K < 20$, taking a color cut of $I-K \pm 0.4$ around the Coma no-evolution line derived for the radio galaxy redshift. For this line, we then determined the equivalent Coma no-evolution redshift. In fitting the red sequence in this manner, we noticed that measuring the slope and scatter of these objects is plagued with systematic errors since the values changed considerably depending on the $I-K$ region used to fit over, with no objective criterion to select the $I-K$ fitting region. For the one radio galaxy without a redshift, MRC 0527$-$255, the dashed line represents a fit of the no-evolution Coma colors to the brightest red galaxies, including the radio galaxy, within the central 35″ and satisfying the color cut $3.6 < I-K < 4.4$. The results are

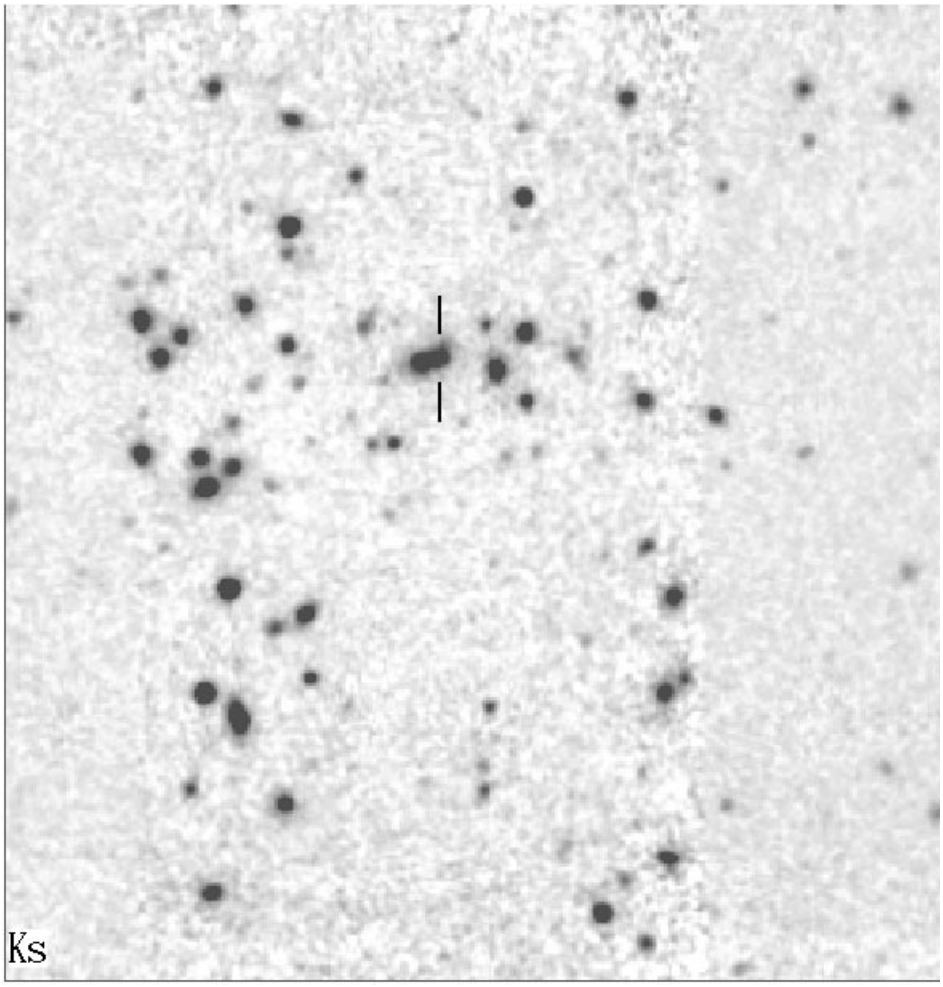

FIG. 3*a*

FIG. 3.—Same as Fig. 1, but for MRC 1022−299 (*a*) *K* and (*b*) *V*; field size 90″ on a side

presented in Table 1 and compared with the measured redshifts of the radio galaxy in the cluster. The uncertainty in the derived redshift results from neglecting to correct for Galactic extinction and from the systematic zero-point uncertainties in the Coma data (which we take as 0.075 mag; Stanford et al. 1998), the photometry, and the choice of objects used for the fit, giving rise to a $\sim$0.10–0.15 mag error for the individual clusters. The $I-K$ red sequence shows a much tighter relation than $V-K$, likely because the extinction is less and the effects of any recent star formation are less pronounced at the longer wavelength.

The case for MRC 0527−255 is less clear than the other three. The $I-K$ red sequence containing the radio galaxy indicates a redshift of $z \sim 1.3$, which would explain the difficulty in measuring a redshift for the radio galaxy with CTIO 4 m blue spectrum. Spectra of the brighter cluster members will be required to verify whether this indeed represents such a high-z cluster.

Certainly for the three radio galaxies with measured redshifts, the location of the expected locus of Coma colors is remarkably consistent with the colors of the red excess galaxies in the field. MRC 0959−263 and MRC 1139−285 do show small color offsets from those expected from the radio galaxy redshift (see § 4). The color difference is measured by the difference at $K = 19$ between the Coma no-evolution line at the radio galaxy redshift and our red-sequence fit line.

3.2. *Individual Clusters*

In this section, we present details of the individual radio galaxy (RG) fields in order of increasing redshift.

3.2.1. *MRC 0959−263*

The $K = 17.7$ radio galaxy lies near the bright end of the red sequence of galaxies, but a $K = 17.0$ elliptical galaxy lying 20″.7 to the northwest may actually be the *brightest cluster member* (BCM) galaxy. The RG has a redshift of $z = 0.68$, but the extrapolated redshift from the red sequence is higher at $z = 0.75$. The no-evolution $I-K$ color difference is $\sim 0.15 \pm 0.10$ mag.

3.2.2. *MRC 1139−285*

This radio galaxy appears to be a likely candidate for the BCM, situated as the brightest galaxy on the red sequence. Another bright red galaxy lying next to the RG on the CMD is actually a barely resolved pair lying 15″ to the northwest. Although the RG has a redshift of $z = 0.85$, the cluster sequence shows very similar colors to MRC 0959−263, with an estimated redshift of $z = 0.77$. This is not very significant against the no-evolution $I-K$ color difference of $\sim 0.18 \pm 0.11$ mag. The cluster members are much more spatially dispersed than in the other three fields, with less obvious central overdensity surrounding the RG.

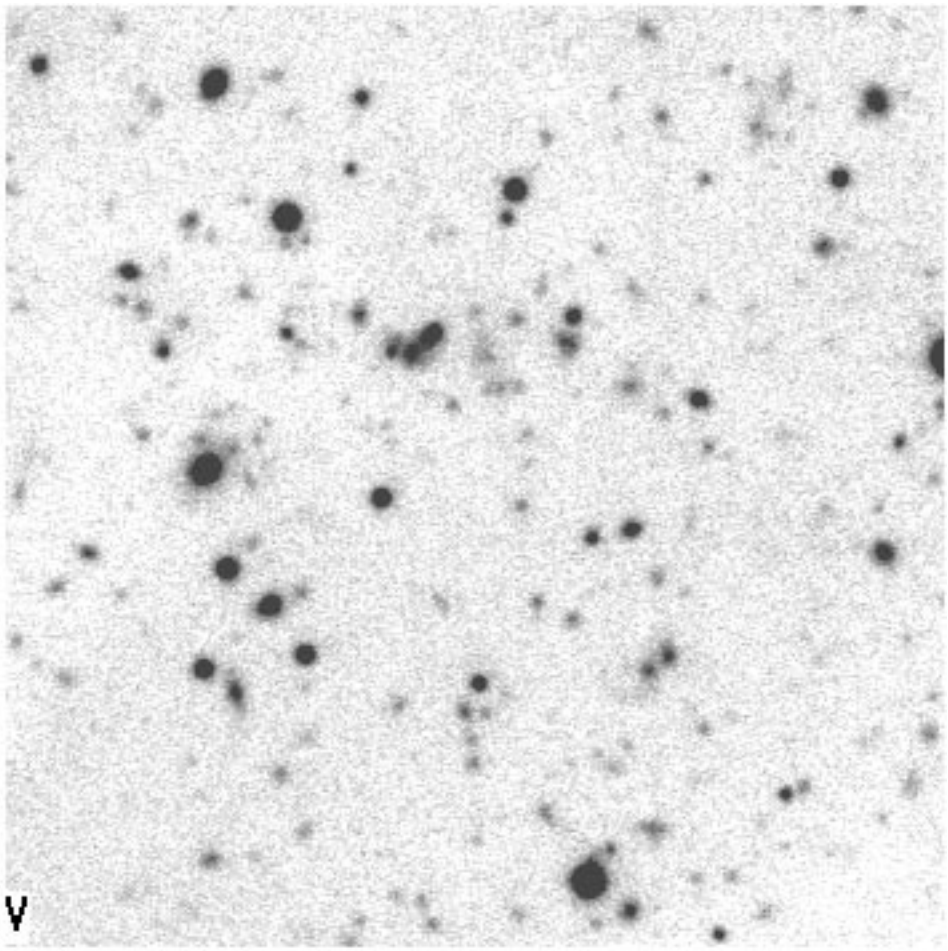

FIG. 3*b*

3.2.3. *MRC 1022−299*

A false-color image of MRC 1022−299 (Fig. 5) shows the dramatic overdensity of red galaxies, the most obvious overdensity from our sample of four radio galaxy fields. This is also apparent in the clear pileup of galaxies along the red sequence in the CMD (Fig. 7). The red sequence, with an estimated redshift $z = 0.95$, clearly includes the RG. The cluster redshift, estimated from the red sequence, is slightly higher than the spectroscopic redshift of the RG itself ($z = 0.93$). The radio galaxy is not the BCM, with the actual BCM on the red sequence ($K_s = 17.8$) lying 38″ from the RG.

3.2.4. *MRC 0527−255*

Although no redshift was measured for the radio galaxy MRC 0527−255, the K-redshift relation for radio galaxies (e.g., Lilly 1989; McCarthy 1993) and the 8″ aperture K magnitude of 17.2 implies $z \sim 1.2$, a higher redshift than the other RGs in the present sample. However, the K-z relation has significant scatter ($dz \sim 0.3$ rms at $z = 1.2$), and it would not be surprising to find the RG and its associated overdense environment at a somewhat lower redshift.

The radio galaxy is among the brightest members of a loose sequence of galaxies with very red colors, where the estimated sequence redshift would be $z = 1.28$. Comparison with the two clusters at similar redshift discovered by Rosati et al. (1999) and Stanford et al. (1997) shows very similar colors in all bands, lending plausibility to this field's representing a high-redshift ($z > 1$) cluster.

In Figure 8, we plot the measured flux converted to AB magnitudes in all known bands of the six K-brightest objects lying on the red sequence within the central 35″ radius of the RG. The K-band flux for all galaxies has been normalized to that of the RG. Overplotted are Coleman, Wu, & Weedman (1980) elliptical galaxy models redshifted to $z = 0.8$, 1.3, and 2.0. The templates at least suggest that if these objects are old cluster members, they lie at redshifts greater than $z = 1$ and are consistent with a cluster lying at $z = 1.3$.

3.3. *Radial Density*

Having identified apparent red sequences from the CMD in all four candidate clusters, we can explore the density of the fields as a function of radius from the radio galaxy. The galaxy density was calculated in successive annuli 5″ wide for each cluster and for the average of all four clusters together (Fig. 9*a*). Figure 9*a* clearly shows a significant excess above the field galaxy limit at our survey depth, $K_s = 20.5$ (*solid horizontal line*; 1 σ errors due to variation in counts across the field are shown as dashed lines—Cowie et al. 1994, 1996; Saracco et al. 1999) for the four clusters averaged together. The average integrated counts over the

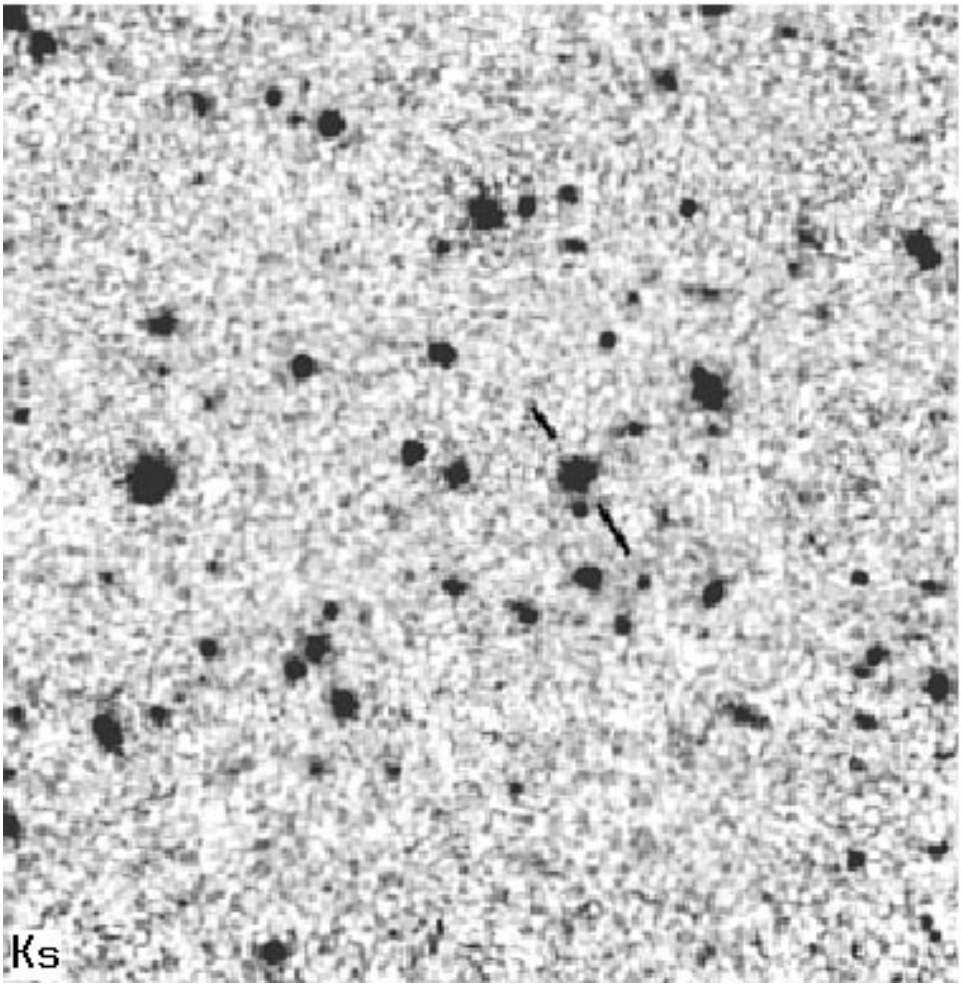

FIG. 4*a*

FIG. 4.—Same as Fig. 1, but for MRC 1139−285 (*a*) K and (*b*) V; field size 90″ on a side

central 25″ radius are more than 6 σ above the field population, estimated conservatively as the field count plus 1 σ. However, the signal in the core region for any cluster on its own is still convincing.

By taking an $I-K$ color cut on the objects of 1 mag bluer than the red sequence in each case (Fig. 9*b*), the significance of the overdensity signal becomes greater, as we have effectively removed a portion of the contaminating field galaxy population (peaking at 65 arcsec^{-2} ≈ 6 σ above the field). However, such a cut also removes all the blue galaxy population residing in the cluster that was bright enough to be detected at K_s band. Cowie et al. (1996) present the counts of field objects of the Hawaii deep surveys with different $I-K$ color cuts. In Figure 9*b*, the field levels are estimated for each cluster using the $K_s = 20.5$ count with an $I-K$ color cut 1 mag bluer than the red-sequence value at $K_s = 19$—the central value of our fitting procedure described in § 3.1. The $I-K$ field limits vary for the clusters from ~ 6 arcmin^{-2} (MRC 0959−263) to ~ 3 arcmin^{-2} (MRC 0527−255). The average of the integrated counts of the respective $I-K$ field limits over the central 25″ radius is a 7.5 σ detected overdensity.

There appear to be two spatial components to the overdensities in all the clusters (Fig. 9). The first is an overdensity within $\sim 30''$ of the RGs relative to our own data at more than 30″ (a *near-field* excess). For all objects with $K_s < 20.5$, this represents a 4.5 σ integrated excess averaged over the four clusters. However, even excluding this near-field excess, the integrated counts for all clusters at radii greater than 30″ relative to random field counts from the literature (Cowie et al. 1996; Saracco et al. 1999) represent a 4.5 σ detection. This *far-field* excess appears to extend to over 80″, although our data are sparse at these radial distances. The amplitude of the near-field excess is insufficient to explain the total excess K_s-band counts, and the far-field excess is likely real. The overdensity in our four fields corresponds to an approximate Abell class of 1.5 ± 0.5, where the red-sequence extrapolated redshift is used in all cases to measure the angular scaling.

3.4. *EROs*

Radio galaxy and quasar fields have shown apparent overabundances of EROs (e.g., Liu et al. 2000; Dey, Spinrad, & Dickinson 1995; McCarthy et al. 1992). The most natural explanation is that these might represent evolved early-type galaxies in a cluster or group environment. Without morphological or submillimeter information, however, it is difficult to know whether any might

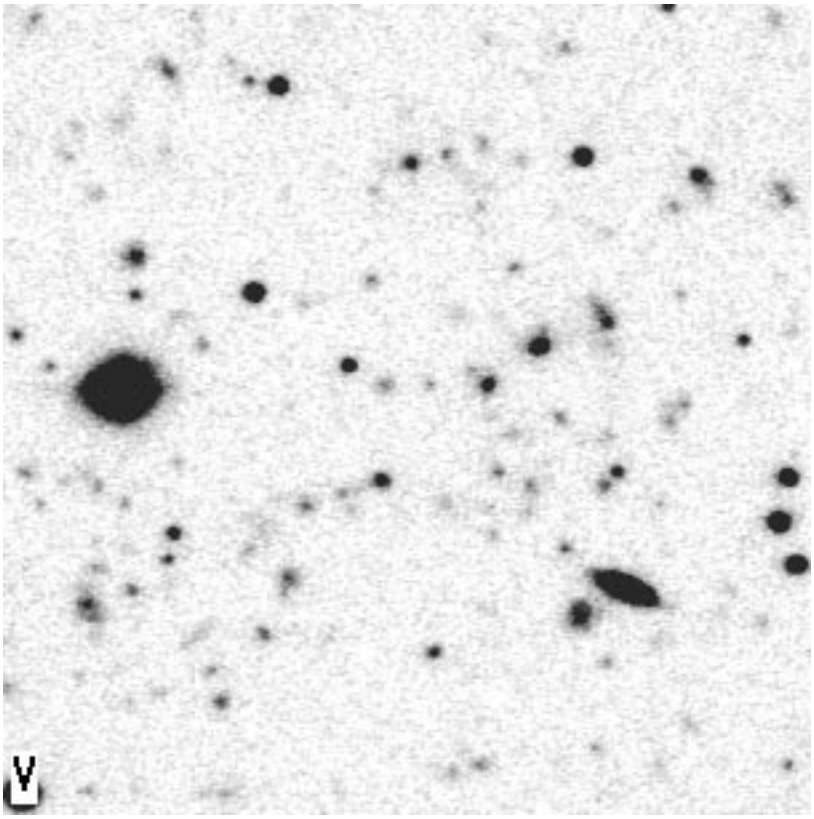

FIG. 4*b*

represent dusty, obscured star-forming objects (Dey et al. 1999; Cimatti et al. 1999). Although all those objects with $I-K>4$ would be considered anomalously red if discovered in the field, in high-z cluster fields they lie close to or along the red galaxy sequence, and their apparent overdensity in our four clusters is large, especially in the two higher redshift fields. However, the objects with $I-K \gtrsim 5$ are clearly too red to form part of the typical mass/metallicity-related sequence of cluster members.

We define two samples of EROs in our RG fields: those with $I-K>5$ and those objects that are significantly above the red sequence ($I-K>4.3$ for the lower redshift clusters, $I-K>4.7$ for the higher redshift clusters). Although many such objects are detected, very few of these objects have $K<19$, and a direct comparison with the random field ERO($R-K>6$) population of Thompson et al. (1999) is difficult. In Table 1, we list the ERO($I-K>5$) and ERO($I-K>$ red seq.) numbers for each cluster to limits of $K<20.0$ (signal-to-noise ratio S/N >5 σ) and $K<20.7$ (S/N >3.5 σ). As some of the candidate EROs appear near the edges of the field, where the exposure time is less than in the central regions, they do not meet our detection criterion of 5 σ and 3.5 σ for the two respective samples, and we do not include these in our catalog. For ERO($I-K>5$), we find 10 and 20 objects in the $K<20.0$ and $K<20.7$ samples, respectively, while for ERO($I-K>$ red seq.), we find 14 ($K<20.0$) and 30 ($K<20.7$) objects. The number of EROs is similar in the four clusters. As the optical magnitudes are very faint in many cases (below our nominal 4 σ detection threshold), all the ERO candidates with $K_s<20$ were verified to be present by visual inspection of the multifilter data. Several of the $K<20.7$ sample were only detected at K_s band.

A field survey using *Hubble Space Telescope* (*HST*) NICMOS data (Yan et al. 2000) derives surface densities of 0.31 ± 0.14 and 0.63 ± 0.2 arcmin^{-2} with $R-H\gtrsim5$ and $H<20.0$ and $H<20.5$, respectively. Yan et al. (2000) liken their $R-H>5$ to $R-K>6$, which has been shown to be roughly equivalent to our $I-K>5$ ERO criterion (Liu et al. 2000). Comparing directly our ERO($I-K>5$) samples with the results of Yan et al., we find surface densities of 0.78 ± 0.25 arcmin^{-2} (2.5 times the field) and 1.41 ± 0.34 arcmin^{-2} (2.2 times the field).

The EROs are not generally within the $\sim35''$ near-field overdensity region, and they tend toward the outer regions of our observed fields (with the possible exception of MRC 0527$-$255). Our candidate EROs are represented as circles in the position-color plots (Fig. 6). This may be indicative of the formation processes that led to the extremely red colors if the EROs are related to the high-z cluster environment. A small percentage of the already overdense old and red cluster galaxies might have enough dust to further redden their colors significantly above the mass/metallicity sequence. Alternatively, there may be an overdensity of dusty ULIRG-type galaxies formed in the dense environment of the radio galaxy. Their location in the outer field excess would be consistent with objects undergoing some phase of merger (see, e.g., van Dokkum et al. 1999). Sensitive submillimeter observations should eventually be able to distinguish between these two possibilities, since the dust mass in the latter case would be substantially larger than for slightly dusty red cluster elliptical galaxies.

FIG. 5.—V-, I-, K-band false-color image of the richest cluster in our sample (120″ on a side), MRC 1022−299. The excess red galaxy population clearly stands out in an already overdense field.

In addition to the above EROs, we also found four objects that originally appeared to be EROs from the $I-K$ color but were found to be bright at V band. Three of these objects appear in the highest redshift field, MRC 0527−255. These objects appear similar to the FROG objects (faint IR-excess field galaxies) discovered by Moustakas et al. (1998) and may represent objects with a nuclear starburst or AGN.

4. DISCUSSION

4.1. *Comparison with Other Clusters*

The magnitude, spatial, and color distributions of the excess galaxy population in these radio galaxy fields are all consistent with the excess being produced by overdensities of galaxies at the RG redshifts. Roughly speaking, the amplitude of the near-field excess corresponds to Abell richness class ∼1 clusters, and the far-field excess to Abell richness ∼1.5. This is consistent with RGs' often being located in large-scale galaxy overdensities and occasionally in smaller scale groups within them. However, the richness measurements should be interpreted cautiously, as one galaxy at $z = 0$ may typically correspond to several galaxies at $z \sim 1$, as a result of mergers in the interim (Steinmetz & White 1997; Stanford et al. 1997).

The objects within 60″ of the radio galaxies at $K < 20$ do not have colors that are significantly different from the no-evolution Coma colors transformed to the redshift of the RG. Because the uncertainty in the zero point of the Coma no-evolution prediction is similar to the amount of expected color evolution in $J-K$ and $H-K$, we would not find strong evidence for passive evolution of the cluster galaxies even without our uncertainties in fitting the red-sequence cluster redshift.

The lack of redshift identifications for cluster members, and the large potential for intervening structure at these relatively high redshifts, makes it difficult to estimate color evolution. We have shown that at least for MRC

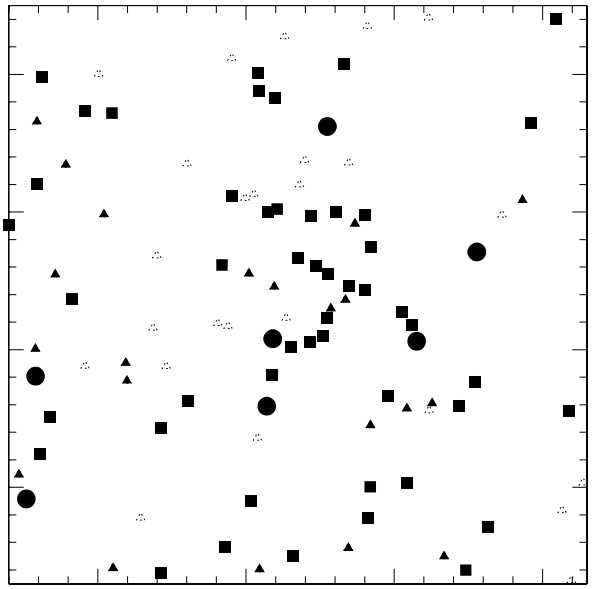

FIG. 6*a*

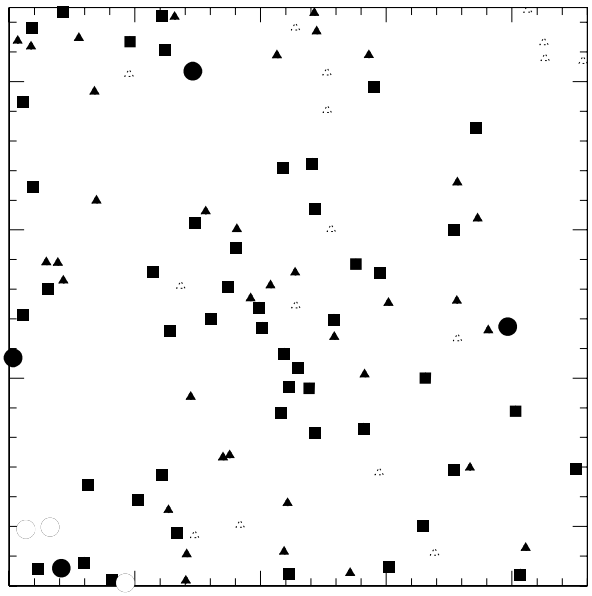

FIG. 6*b*

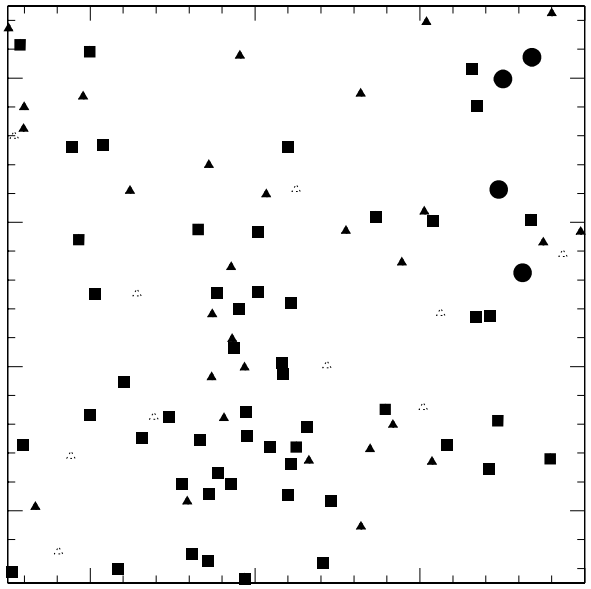

FIG. 6*c*

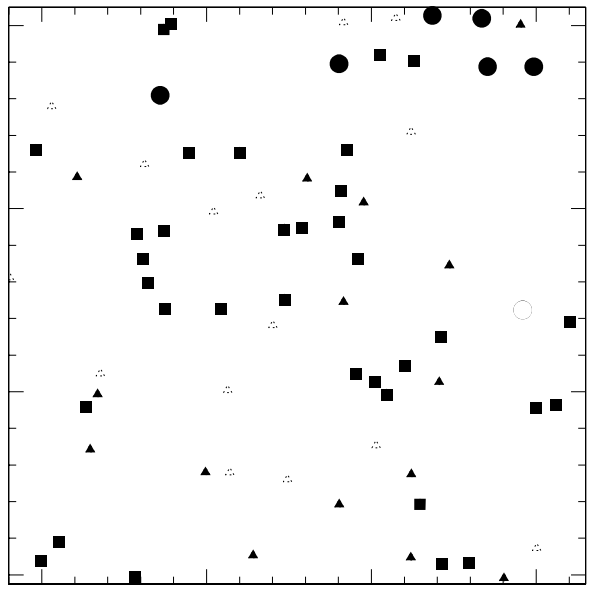

FIG. 6*d*

FIG. 6.—Cluster position-color diagrams, showing the density of red-sequence objects and EROs. The angular extents of the plots are similar to the images in Figs. 1–4. Only objects with a greater than 4 σ detection at K_s band are depicted. (*a*) MRC 0527−255; (*b*) MRC 0959−263; (*c*) MRC 1022−299; (*d*) MRC 1139−285. Squares represent objects lying on the red sequence; filled triangles represent galaxies with $I-K > 1.2$ mag bluer than the red sequence, and open triangles those with $I-K > 2$ mag bluer than the red sequence. EROs with $I-K$ at least 1 mag redder than the respective elliptical sequence are shown with circles (at least $I-K > 4.3$).

1022−299, the red-sequence estimated redshift is very close to the RG redshift itself. For the case of the more dispersed cluster, MRC 1139−285, and the nearest cluster, MRC 0959−263, the red-sequence estimated redshift is somewhat different from that of the RG ($\delta z = 0.08$). Although the radio galaxy redshift is not necessarily the best redshift for the cluster (the RG is not clearly the BCM galaxy in any cluster), a velocity dispersion corresponding to $dz = 0.08$ would be relatively large for clusters at our RG redshifts (Deltorn et al. 1997; van Dokkum et al. 1999; Rosati et al. 1999). It would therefore be surprising if the cluster redshift were systematically offset from that of the RG. In addition, the photometry and Coma zero-point errors added in quadrature ($3\ \sigma \sim 0.2$ mag) are similar to the measured color offsets. Therefore we are reluctant to associate such minor color offsets from the Coma no-evolution colors with excess or diminished cluster evolution. MRC 0527−255 has only the red-sequence estimated redshift to work from, and until spectroscopic redshifts are obtained, nothing further can be gathered about the color evolution.

The colors of most of the objects lying near the red sequence are broadly consistent with the predictions of Bruzual & Charlot (1993) elliptical galaxy models for $z = 0.76$, 0.78, 0.95, and 1.28, respectively, with the following properties: passive evolution of a 1 Gyr burst stellar population with solar metallicity formed at $z = 5$ for

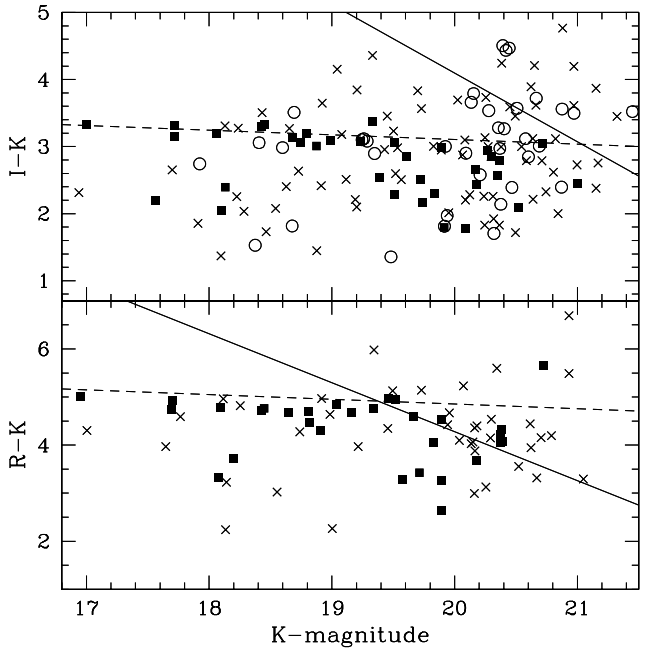

FIG. 7*a*

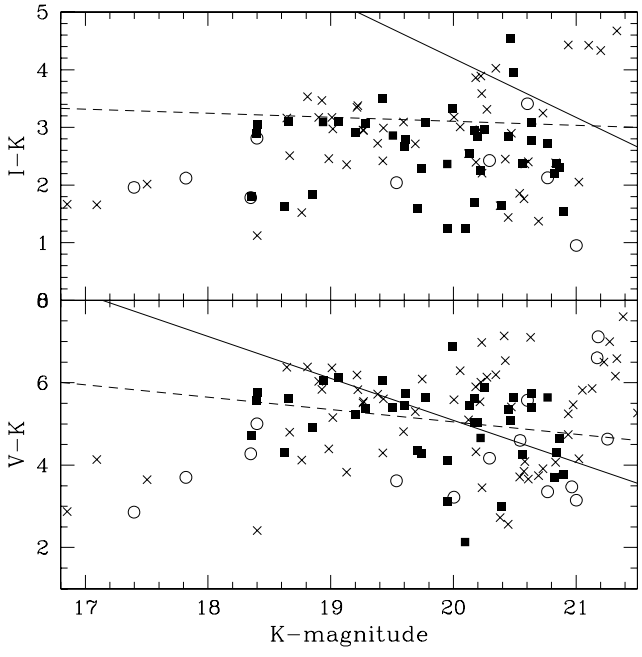

FIG. 7*b*

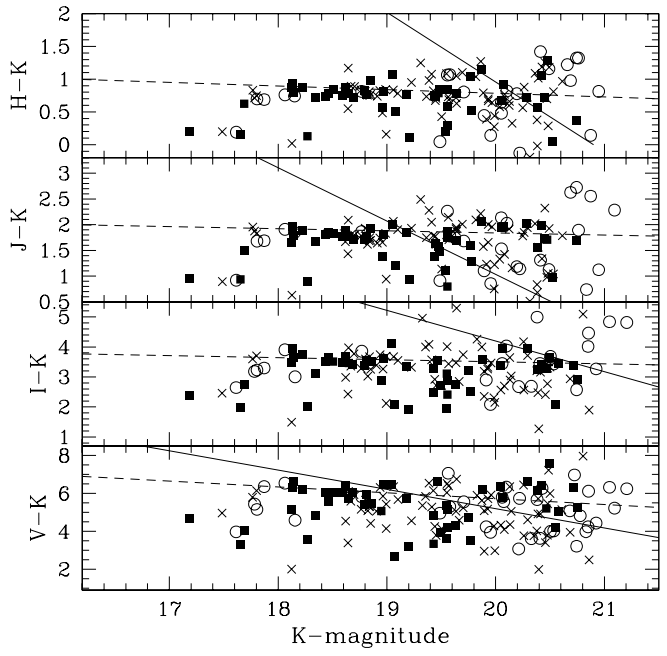

FIG. 7*c*

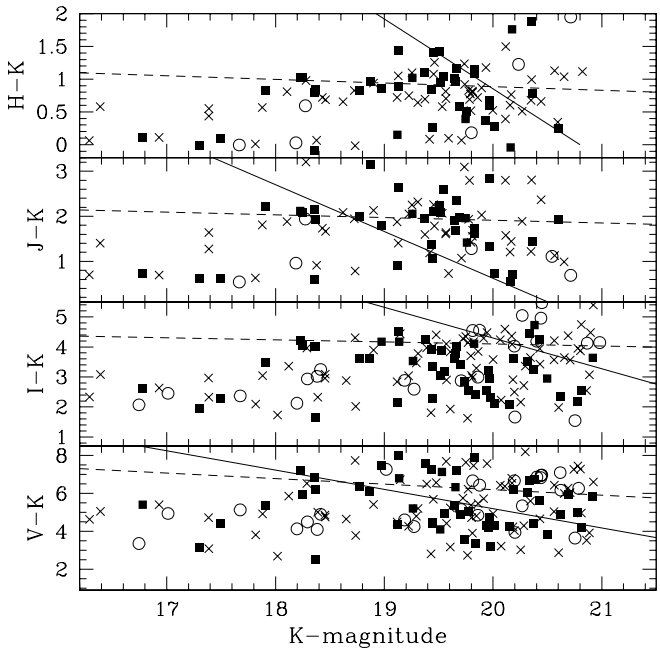

FIG. 7*d*

FIG. 7.—Cluster CMDs at two radial cuts showing the red sequence emerging. In order of increasing redshift, (*a*) MRC 0959−263; (*b*) MRC 1139−285; (*c*) MRC 1022−299; (*d*) MRC 0527−255. Radial cuts have been made on the objects to provide an idea of the color distributions with distance from the radio galaxy. Filled squares represent objects within 35″ of the radio galaxy, crosses those from 35″ to 60″, and circles those from 60″ to 90″. Dashed lines depict the locus of Coma Cluster colors transformed to the redshift of the RG-selected cluster. The solid diagonal lines represent 4 σ detection thresholds in color, with magnitude errors added in quadrature. Note that for MRC 0959−263, the Gunn *r*-band image covers a somewhat smaller area than the *I* and *K* images, and many of the galaxies identified in the *I* and *K* fields are not present in *r*.

$h = 0.65$ and $q_0 = 0.1$. For our most distant possible cluster (MRC 0527−255; $z = 1.28$), such a model predicts $V-K = 7.0$, $I-K = 4.3$, and $J-K = 1.9$ for a galaxy age of 3.25 Gyr. It is noteworthy that the same "standard" passive evolution model was also found to provide a reasonable fit to the average optical-IR colors of early-type galaxies in the large sample of rich optically and X-ray–selected clusters at $0.3 < z < 0.9$ (Stanford et al. 1998). Ages less than $\sim$3 Gyr for the stellar populations could be accommodated if the mean metallicity were greater than solar. Also, we have made no attempt to correct the colors for extinction due to dust internal to the galaxies. If this is large, then the true colors of the cluster galaxies would be bluer than our measured values, resulting in a better fit to models with $z_f < 3$.

The apparent scatter and slope of the red sequence can be used as a measure of the relative mix of stellar populations present in these early epoch cluster ellipticals. Our lack of

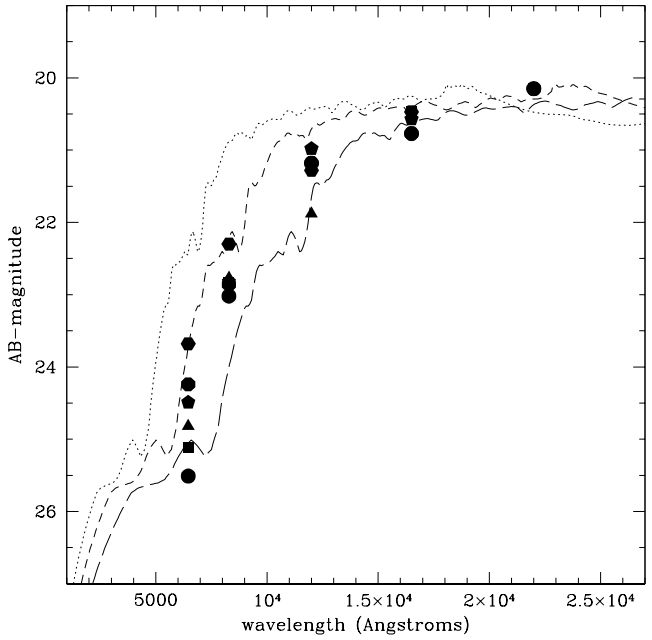

FIG. 8.—MRC 0527−255: spectral energy plot of the six K-band brightest galaxies lying along the assumed red sequence for the cluster. The lines represent an elliptical galaxy redshifted and k-corrected to $z = 0.8$ (*dotted line*), $z = 1.0$ (*short-dashed line*), and $z = 1.28$ (*long-dashed line*). Although evolutionary effects will make this model spectral energy distribution less red, dust effects would considerably redden the profile, providing a better fit to the data at wavelengths shortward of 1 μm. These six red objects provide some indication that the cluster likely does lie at $z > 1$.

morphology selection from high spatial resolution (i.e., *HST*) images makes color-scatter comparisons difficult, since we have inadvertently removed all bluer galaxies from consideration as cluster members. Stanford et al. (1998) noted no significant increase in red-sequence scatter to $z \sim 0.9$ using *HST*-selected E+S0 galaxies in clusters. Beyond $z = 1$, the mix of stellar populations is expected to increase the scatter and slope (Kodama et al. 1998), leaving a clear excess of red galaxies but a much looser "sequence." This appears to be the case in two recent analyses of AGN-selected clusters: 3C 324, at $z = 1.206$ (Kajisawa et al. 2000), and B2 1335+28, at $z = 1.11$ (Tanaka et al. 2000). However, the $z \sim 1.3$ clusters discovered in the Lynx IR field survey, RX J0848.9+4452 and CIG J0848+4453 (Rosati et al. 1999), still show a relatively tight red sequence. Our apparent red-sequence scatter and slope out to $z \sim 0.9$ appear similarly to the eye to that found by Stanford et al. (1997), but we do not attempt to quantify the slope or scatter as described in § 3.1. MRC 0527−255, possibly at $z \sim 1.3$, does show a rather loose red sequence similar to that of 3C 324, although the pileup of red objects at fainter magnitudes is fraught with photometric errors, and it is not clear which objects to include in the sequence.

4.2. *Connections with the Radio Galaxy*

These four clusters are clearly among the highest density environments in our total sample of high-z radio galaxies (Chapman & McCarthy 2000). The radio power and source structure vary significantly through the four RGs, even after

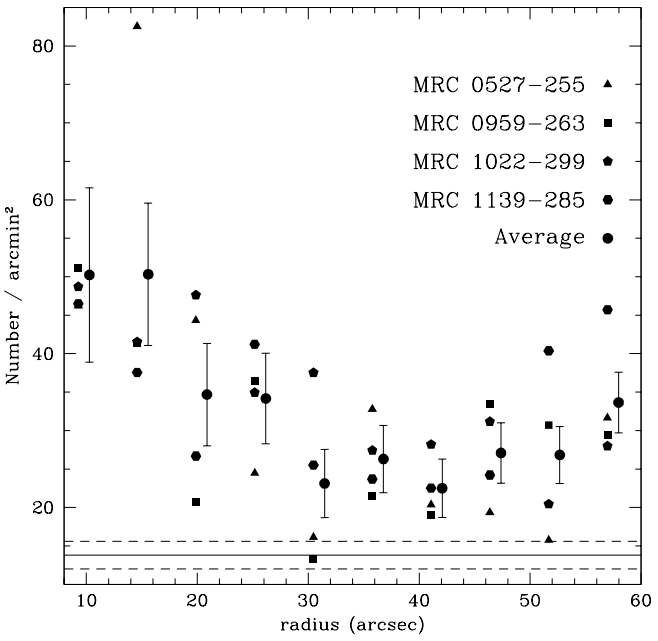

FIG. 9*a*

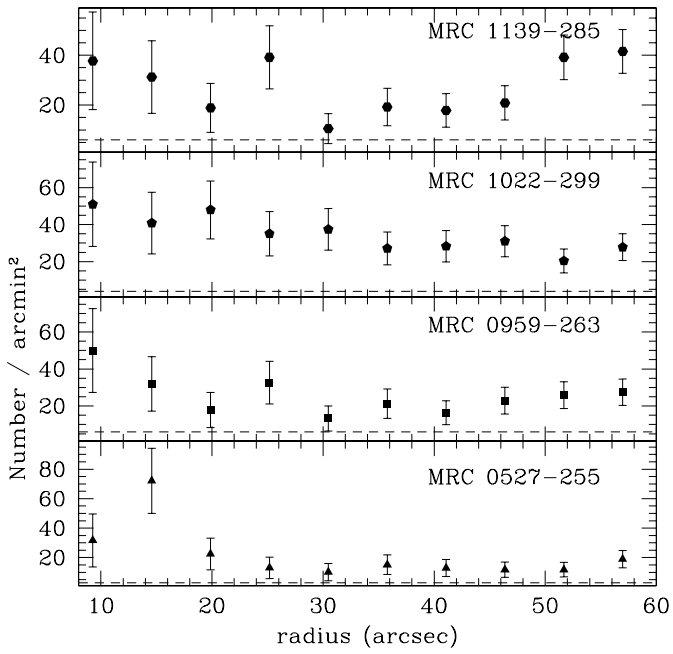

FIG. 9*b*

FIG. 9.—(*a*) Projected radial distribution of all galaxies brighter than $K_s = 20.5$ (2″ aperture diameter) within the average of the four clusters (*circles*), with error bars calculated for the number of objects in each bin as per Gehrels (1986). The individual clusters are also plotted, slightly offset in radius for clarity. A clear signal is seen as a significant excess above the field galaxy limit at our K_s-band survey depth (*solid horizontal line*; 1 σ error bars as dashed lines). (*b*) By making a color cut on the objects of 1 mag bluer than the $I-K$ red sequence in each case, the strength of the overdensity signal becomes even larger, as we have cut out a portion of the contaminating field galaxy population. The $I-K$ color-cut limits for the field in each case are taken from Cowie et al. (1996; *horizontal dashed lines*) and vary from ~ 6 arcmin^{-2} (MRC 0959−263) to ~ 3 arcmin^{-2} (MRC 0527−255). Again, the error bars are calculated for the number of bins as per Gehrels (1986).

accounting for redshift differences (Table 1). However the spectral index ($\alpha_{843/408}$) is similar for the four objects, placing them all slightly shallow of the steep-spectrum source definition ($\alpha > 0.9$) from Kapahi et al. (1998). The relatively steep spectrum is typical for distant RGs (McCarthy 1993). The RG is not clearly the BCM galaxy in any of the clusters (although it is one of the two or three obviously brightest sequence members in MRC 0527−255 and MRC 1139−285). This may be expected if the formation and evolution of the RG depend, for instance, only on a few trigger merger events early in the cluster formation period. The RG properties would then only loosely relate to the local environment.

Although early suggestions that nuclear properties and radio source structure are linked to the clustering environment (Heckman et al. 1986), we find no obvious evidence for environmental differences in our cluster fields over those selected through X-ray or optical techniques. Higher merger rates might be expected to associate with high-z RG cluster environments, especially those less rich clusters with smaller velocity dispersions (see, e.g., Barnes 1999). However, direct studies of merger fractions are difficult without higher resolution imagery, and blue fractions of clusters at high z are difficult to quantify because of the strong variation in the blue field population in the foreground (Ellis 1997). Our clusters do all show a compact environment present in the central $\sim 35''$ that is somewhat distinct from richer X-ray–selected clusters at similar redshifts (van Dokkum et al. 1999; Rosati et al. 1999). This may indicate a locally higher merger environment in the cluster center than typical (by contrast, van Dokkum et al. 1999 found higher merger fractions in the outer radii of the clusters through *HST* imaging of close pairs). It remains to be seen whether there is any true correlation of cluster and radio properties in a large flux-limited sample.

5. CONCLUSIONS

The observations presented here provide strong evidence supporting the cluster identification for the very red galaxy overdensities in the environments of these four radio galaxies' environments. The density of all objects within $25''$ radius of the radio galaxy field centers is ~ 6 times higher than the field average. Excluding the bluer objects, the overdensity peaks at ~ 7.5 times the field count subjected to similar $I-K$ color cuts.

The quiescent behavior of early-type galaxies in clusters to $z \sim 1$ appears to represent the evolutionary history of these RG-selected clusters fairly well. The picture of smooth and steady evolution has been demonstrated with only a handful of relatively rich clusters selected through the X-ray and optical morphology thus far, and our four clusters add significant evidence to this picture.

No clear connection exists in our data between the radio galaxy properties and the clustering environment, except for the local peak in the overdensity surrounding the radio galaxy.

We thank the staff of the Las Campanas Observatory, and F. Peralta and H. Olivares, in particular, for their assistance with the observations. We also thank D. Murphy for technical assistance with IRCAM, and M. Beckett, D. Murphy, and R. McMahon for technical assistance with CIRSI. The referee helped us to improve the final version by providing a valuable critique of the submitted version of this paper.

REFERENCES

Barnes, J. E. 1999, in ASP Conf. Ser. 187, The Evolution of Galaxies on Cosmological Timescales, ed. J. E. Beckman & T. J. Mahoney (San Francisco: ASP), 463
Beckett, M. G., Mackay, C. D., McMahon, R. G., Parry, I. R., Ellis, R. S., Chan, S. J., & Hoenig, M. 1998, Proc. SPIE, 3354, 431
Bertin, A., & Arnouts, S. 1996, A&AS, 117, 393
Boyle, B. J., & Terlevich, R. J. 1998, MNRAS, 293, L49
Bruzual A., G., & Charlot, C. 1993, ApJ, 405, 538
Chapman, S. C., & McCarthy, P. J. 2000, in preparation
Cimatti, A., Andreani, P., Röttgering, H., & Tilanus, R. 1998, Nature, 392, 895
Coleman, G. D., Wu, C.-C., & Weedman, D. W. 1980, ApJS, 43, 393
Cowie, L. L., Gardner, J. P., Hu, E. M., Songaila, A., Hodapp, K.-W., & Wainscoat, R. J. 1994, ApJ, 434, 114
Cowie, L. L., Songaila, A., Hu, E. M., & Cohen, J. G. 1996, AJ, 112, 839
Deltorn, J.-M., Le Fèvre, O., Crampton, D., & Dickinson, M. 1997, ApJ, 483, L21
Dey, A., Graham, J. R., Ivison, R. J., Smail, I., Wright, G. S., & Liu, M. C. 1999, ApJ, 519, 610
Dey, A., Spinrad, H., & Dickinson, M. 1995, ApJ, 440, 515
Eisenhardt, P., & De Propris, R. 1997, BAAS, 190, No. 3.04
Ellingson, E., Yee, H. K. C., & Green, R. F. 1991, ApJ, 371, 49
Ellis, R. S. 1997, ARA&A, 35, 389
Ellis, R. S., Smail, I., Dressler, A., Couch, W. J., Oemler, A., Jr., Butcher, H., & Sharples, R. M. 1997, ApJ, 483, 582
Fabian, A. C., & Crawford, C. S. 1990, MNRAS, 247, 439
Gehrels, N. 1986, ApJ, 303, 336
Gladders, M. D., López-Cruz, O., Yee, H. K. C., & Kodama, T. 1998, ApJ, 501, 571
Hall, P. B., & Green, R. F. 1998, ApJ, 507, 558
Heckman, T. M., Smith, E. P., Baum, S. A., van Breugel, W. J. M., Miley, G. K., Illingworth, G. D., Bothun, G. D., & Balick, B. 1986, ApJ, 311, 526
Hill, G. J., & Lilly, S. J. 1991, ApJ, 367, 1
Kajisawa, M., et al. 2000, PASJ, 52, 61
Kapahi, V. K., Athreya, R. M., Subrahmanya, C. R., Baker, J. C., Hunstead, R. W., McCarthy, P. J., & van Breugel, W. 1998, ApJS, 118, 327
Kauffmann, G., & Charlot, S. 1998, MNRAS, 294, 705
Kodama, T., Arimoto, N., Barger, A. J., & Aragón-Salamanca, A. 1998, A&A, 334, 99
Lilly, S. J. 1989, ApJ, 340, 77
Lilly, S. J., & Prestage, R. M. 1987, MNRAS, 225, 531
Liu, M. C., Dey, A., Graham, J. R., Bundy, K. A., Steidel, C. C., Adelberger, K., & Dickinson, M. E. 2000, AJ, 119, 2556
McCarthy, P. J. 1993, ARA&A, 31, 639
McCarthy, P. J., et al. 2000, in preparation
McCarthy, P. J., Elston, R., & Eisenhardt, P. 1992, ApJ, 387, L29
McCarthy, P. J., Kapahi, V. K., van Breugel, W., Persson, S. E., Athreya, R., & Subrahmanya, C. R. 1996, ApJS, 107, 19
Moustakas, L. A., Davis, M., Zepf, S. E., & Bunker, A. J. 1998, in ASP Conf. Ser. 146, The Young Universe: Galaxy Formation and Evolution at Intermediate and High Redshift, ed. S. D'Odorico, A. Fontana, & E. Giallongo (San Francisco: ASP), 210
Persson, S. E., West, S. C., Carr, D. M., Sivaramakrishnan, A., & Murphy, D. C. 1992, PASP, 104, 204
Press, W. H., & Schechter, P. 1974, ApJ, 187, 425
Rosati, P., Stanford, S. A., Eisenhardt, P. R., Elston, R., Spinrad, H., Stern, D., & Dey, A. 1999, AJ, 118, 76
Saracco, P., D'Odorico, S., Moorwood, A., Buzzoni, A., Cuby, J.-G., & Lidman, C. 1999, A&A, 349, 751
Stanford, S. A., Eisenhardt, P. R., & Dickinson, M. 1998, ApJ, 492, 461
Stanford, S. A., Elston, R., Eisenhardt, P. R., Spinrad, H., Stern, D., & Dey, A. 1997, AJ, 114, 2232
Steidel, C. C., Adelberger, K. L., Giavalisco, M., Dickinson, M., & Pettini, M. 1999, ApJ, 519, 1
Steinmetz, M., & White, S. D. M. 1997, MNRAS, 288, 545
Tanaka, I., Yamada, T., Aragón-Salamanca, A., Kodama, T., Miyaji, T., Ohta, K., & Arimoto, N. 2000, ApJ, 528, 123
Thompson, D., et al. 1999, ApJ, 523, 100
van Dokkum, P. G., Franx, M., Fabricant, D., Kelson, D. D., & Illingworth, G. D. 1999, ApJ, 520, L95
Yan, L., McCarthy, P. J., Weymann, R. J., Malkan, M. A., Teplitz, H. I., Storrie-Lombardi, L. J., Smith, M., & Dressler, A. 2000, AJ, 120, 575
Yates, M. G., Miller, L., & Peacock, J. A. 1989, MNRAS, 240, 129
Yee, H. K. C., & Green, R. F. 1984, ApJ, 280, 79